Title
A New Wideband Spread Target Maximum Likelihood Estimator for Blood Velocity Estimation: Part One - Theory

Journal
IEEE Transactions on Ultrasonics, Ferroelectrics and Frequency Control, 38

Authors
Ferrara, K. Whittaker
Algazi, Ralph

Publication Date
1991

Peer reviewed

T-UFFC/38/1//40244

A New Wideband Spread Target Maximum Likelihood Estimator for Blood Velocity Estimation Part I: Theory

Katherine W. Ferrara
V. Ralph Algazi

Reprinted from
IEEE TRANSACTIONS ON ULTRASONICS, FERROELECTRICS, AND FREQUENCY CONTROL
Vol. 38, No. 1, January 1991

A New Wideband Spread Target Maximum Likelihood Estimator for Blood Velocity Estimation—Part I: Theory

Katherine W. Ferrara, *Member, IEEE*, and V. Ralph Algazi, *Senior Member, IEEE*

Abstract—**The derivation and theoretical evaluation of new wideband maximum likelihood strategies for the estimation of blood velocity using acoustic signals are presented. A model for the received signal from blood scatterers, using a train of short wideband pulses, is described. Evaluation of the autocorrelation of the signal based on this model shows that the magnitude, periodicity and phase of the autocorrelation are affected by the mean scatterer velocity, and the presence of a velocity spread target. New velocity estimators are then derived that exploit the effect of the scatterer velocity on both the signal delay and the shift in frequency. The wideband range spread estimator is derived using a statistical model of the target. Based on the point target assumption, a simpler wideband maximum likelihood estimator is also obtained. These new estimation strategies are analyzed for their local and global performance. Evaluation of the Cramer-Rao bound shows that the bound on the estimator variance is reduced using these estimators, in comparison with narrowband strategies. In order to study global accuracy, the expected estimator output is evaluated, and it is determined that the width of the mainlobe is reduced. In addition, it is shown that the height of subsidiary velocity peaks is reduced through the use of these new estimators.**

NOMENCLATURE

A_i	Scattering amplitude of the ith scatterer.
α	Beam vessel angle.
$b[r(t)]$	Lateral beam weighting, a function of radial position and time.
β	Axial velocity of scatterers under the SFPT assumption.
c	Acoustic propagation velocity.
d	Delay used in the estimator structure.
d	Two way travel time to the center of the target.
$\mathcal{E}[$	Expected value.
E_r	Energy in the returned signal, defined by (50).
E_t	Filtered transmitted energy in a single envelope $s'(\ )$.
$\mathcal{F}[\ ]$	Fourier transform operator.
ϕ_l	$=2lT/c$.
$h'(t, u; v)$	Linear filter defined in (5).
$h'_{as}(t)$	Linear filter which models the effect of intervening and scattering media.
$\theta(\ )$	Spread target ambiguity function.
$l(v)$	Likelihood function of velocity v.
N_o	Noise power.
P	Number of pulses transmitted.
$q(\ )$	Generalized ambiguity function.
$r(t)$	Received signal.
$r'(t)$	Complex envelope of the received signal.
$R_r(t, u)$	Complex autocorrelation of the envelope of the received signal.
$R_s[\ ]$	Defined by (11).
$s'(t - 2z/c$	Deterministic filtered complex envelope from a depth z.
σ	$=2w_o/c$.
T	Period of the transmitted pulse.
$v(r)\cos\alpha$	Axial velocity of scatterers located at coordinate r.
	Axial velocity parameter used in nonfluctuating MLE.
w	Radial frequency.
w_o	Center frequency of the transmitted pulse.
$w_1($	Data window for the wideband range spread MLE.
w_2	Signal correlation window, includes lateral beam modulation and velocity variations.

Manuscript received July 3, 1989; revised July 13, 1990; accepted July 16, 1990.

K. W. Ferrara is with the Department of Electrical and Electronic Engineering, California State University, Sacramento, CA 95819, and with the Center for Image Processing and Integrated Computing (CIPIC), University of California, Davis, Davis, CA 95616.

V. R. Algazi is with the Center for Image Processing and Integrated Computing (CIPIC) and with the Department of Electrical Engineering and Computer Science, University of California, Davis, Davis, CA 95616.

IEEE Log Number 9040244.

I. INTRODUCTION

NEW MAXIMUM likelihood estimation strategies for blood velocity, using acoustic signals of high fractional bandwidth and based on a model that describes the spread nature of the target are presented. These processing strategies utilize both the change in scatterer position and the change in frequency of the returned signal. This approach leads to improvements in performance that can be shown through improved local and global accuracy of the estimator.

The utilization of the change in scatterer position *and* the change in the frequency of the returned signal provides a theoretical link between previous analysis of the Doppler shift of the returned signal [1]–[4] and recent research into the use of time-domain correlation for velocity estimation [5]–[8]. Through this theoretical link, we show that the local accuracy is improved using the new joint strategy, in comparison with previous approaches.

In blood velocity estimation the goal is to measure the velocity distribution within the smallest region possible and to repeat this measurement quickly and accurately over the entire region of interest. Therefore, as in other estimation problems, the joint optimization of spatial, velocity and temporal resolution is critical. In this new strategy, periodic wideband signals are trans-

0885-3010/91/0100-0001$01.00

mitted and small volumes are illuminated. Using the new estimators, we will show that these volumes can be tracked, each for an interval that can be independently optimized. Thus, using these estimators, appropriate signal processing parameters can be determined for each region of the scattering medium, utilizing the local velocity distribution. Optimal parameters for these estimation strategies are discussed.

The evaluation of the performance of these estimators leads to several new results. We first examine the local accuracy by the use of the Cramer–Rao bound and find a new form of the variance. The study of global accuracy requires a generalization of the ambiguity function that allows for the wideband illumination of a spread target. With the selection of appropriate operating parameters, the new wideband maximum likelihood estimators are shown to be superior to current strategies in variance or local accuracy, in velocity resolution, and in diminished subsidiary velocity peaks.

The theoretical conclusions of this paper are verified with experimental data in Part II [19]. In addition, using these estimators, we demonstrate that the spatial-velocity profile can be estimated across the vessel.

A. Previous Strategies

Most previous theoretical discussion of blood velocity estimation has assumed a narrowband transmitted signal, which leads to the approximation of the returned signal as a frequency shifted version of the transmitted signal. Although this approximation simplifies analysis, it discards valuable information in the envelope of the signal. In addition, narrowband signal transmission combined with a narrowband estimation strategy produces resolution limitations. Using a narrowband estimation strategy, the limit on the velocity resolution is determined by the transit time of individual scatterers moving through the sample volume, which is frequently constrained by the axial pulse length [3]. Since the axial pulse length is determined by the narrowband transmitted signal, the axial spatial resolution is identical in all axial regions, and therefore the spatial-velocity resolution product will depend on the transit time of each group of scatterers, and thus on their velocity. This product is not generally optimized for the velocity of the scatterers and cannot be optimized for multiple velocity components encountered in individual axial regions. In addition, signal and thus velocity aliasing is a frequent problem.

Other recent research in the area of blood velocity estimation has included time shift correlation, and it has been shown that the delay of the returned signal can be used to estimate the velocity of the scatterers. The estimation strategies used within this paper incorporate information in both the delay and phase of the signal which independently form the bases of previous strategies.

B. Organization

Our paper is organized as follows. In order to develop wideband estimation strategies, a model is developed which describes the returned signal from wideband illumination of a range and velocity spread target, frequently referred to as a doubly spread target. The model and statistics for the received signal are presented in Sections II and III. This model describes the received signal from a moving group of scatterers for a transmitted signal that consists of a periodic series of short wideband pulses. Since the true scattering medium in blood is distributed in range and velocity and the transmitted pulse has a finite dimension, the effect of the medium on the pulse envelope is also included. The slowly fluctuating point target (SFPT) model, utilized in most previous research, is used for comparison.

The general estimator for a spread target and a simpler form based upon the point target approximation are derived in Section IV using the maximum likelihood approach. The consideration of the range spread nature of the target increases the complexity of the estimator but is shown to improve the estimator performance. The resulting strategy is referred to as the wideband range spread maximum likelihood estimator. In addition, a simpler estimator based upon the SFPT approximation is proposed and referred to as the wideband point maximum likelihood estimator. The term wideband MLE (WMLE) is used to refer to the common properties of both estimators. Although the use of a wideband signal reduces the sample volume size and therefore the spread of velocity components illuminated, in some cases the illuminated target remains velocity spread. Using the new strategies, the velocity distribution and its moments can be estimated for each spatial region in the vessel.

The performance of these estimators is then considered. The local accuracy is evaluated in Section V using the Cramer–Rao bound. Finally, the global accuracy is considered in Section VI through the evaluation of the width of the mainlobe and the height of subsidiary velocity peaks.

II. Model for the Received Signal From a Target

We utilize a model for the received signal resulting from illumination of the target with a signal of significant fractional bandwidth. The model used in this analysis is similar to the model described by Atkinson [2], but differs due to the transmission of a periodic signal of significant fractional bandwidth. This model is derived in detail in Ferrara [10] and has the important feature that both the period of the envelope and the center frequency of the returned signal contain information concerning the velocity of the target, and can be used in velocity estimation.

In this strategy, the pulse repetition period T is much longer than the pulse duration, and the compression or expansion of the *individual* envelope can be ignored. Under this constraint, the effect of the scatterer velocity on the envelope is approximated by a change in the pulse repetition period, and this change is proportional to the axial component of the velocity of the scatterer.

The model for the blood scattering medium requires specific statistical assumptions in order to describe random amplitude variations in the returned signal. The scattering elements are assumed to consist of small aggregates of red blood cells with random aggregate size. The position of the ith scatterer at time $t = 0$, is also considered to be random, with a uniform distribution in a scattering medium which is large with respect to the sample volume. The amplitude of the summed returned signal from all scatterers is assumed to display a Gaussian distribution. The movement of the scatterers is considered to be a deterministic function of scatterer position.

Let us now define the coordinate systems to be used in this analysis. As shown in Fig. 1, two cylindrical coordinate systems are defined. One system describes the ultrasonic beam, the other system describes the vessel. For the vessel coordinate system, $\tilde{z}$, $\tilde{r}$, and $\tilde{\Phi}$ represent the cylindrical coordinates. For the beam coordinate system, z, r, and Φ represent the cylindrical coordinates. The origins of the beam and vessel coordinate system are offset by a distance $cd'/2$ along the z axis. The angle between the axes z, and $\tilde{z}$ is given by α.

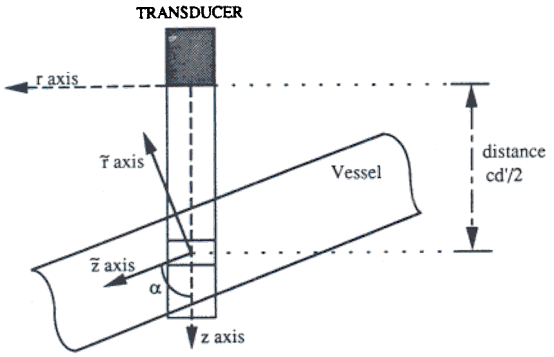

Fig. 1. Beam and vessel cylindrical coordinate systems, where $\tilde{z}$ and $\tilde{r}$ are the axial and radial coordinates of the vessel, and z and r are the axial and radial coordinates of the beam.

We now discuss a few additional simplifications and establish our notation. The notation is summarized in the Nomenclature section.

The model for the deterministic envelope of the returned signal allows for the effect of frequency dependent attenuation and the frequency dependence of the scattering function on the complex envelope by modelling these effects using the linear filter $h'_{as}(t, z)$. This model has been derived for narrowband signals by Holland in [11], and for wideband signals in [10]. First, let $f'(t)$ represent the complex envelope of the transmitted signal, filtered by the impulse response of the transducer on transmission and reception. Then, the deterministic, filtered complex envelope received from a depth z is represented by $s'(t - 2z/c)$, where $s'(t)$ is the result of the convolution of $f'(t)$ with $h'_{as}(t, z)$. Letting ψ denote the attenuation constant of the tissue, $h'_{as}(t, z)$ is the inverse Fourier transform of the quantity $\{(w^2/2z) \exp[-\psi w z]\}$. We choose to normalize $s'(t)$ such that $\int |s'(t)|^2 dt$ over infinite limits equals one, and E_t represents the filtered transmitted energy.

The complete model for the received signal consists of the sum of terms over scatterers indexed by i and pulses or periods indexed by k. These terms are scaled by the amplitude A_i of the signal from each scatterer, and include the lateral beam sensitivity $b[r_i(t)]$ of the ith scatterer, the delayed deterministic envelope s', the phase of the signal from each scatterer, and the Doppler shift.

Under the assumption of laminar flow and taking into account the angle, α, between the vessel and the beam, we obtain the following expression:

$$r'(t) \approx \sqrt{E_t} \sum_i \sum_k A_i b[r_i(t)] \cdot s'\left[t - 2z_i/c - kT/\{ - 2v(\tilde{r}_i \cos\alpha/c\}\right] \cdot \exp\left[-j\sigma(z_i + v(\tilde{r}_i)\cos\alpha \cdot t)\right]. \quad (1)$$

Since $1/\{1 - x\} \approx 1 + x$ for $x \ll 1$ with $x = 2v(\tilde{r}_i)\cos\alpha/c$, we make the further approximation:

$$r'(t) \approx \sqrt{E_t} \sum_i \sum_k A_i b[r_i(t)] \cdot s'\left[t - 2z_i/c - kT\{1 + 2v(\tilde{r}_i)\cos\alpha/c\}\right] \cdot \exp\left[-j\sigma(z_i + v(\tilde{r}_i)\cos\alpha \cdot t)\right]. \quad (2)$$

We note that both the period of the envelope and the center frequency of the returned signal contain information about the velocity of the target. The total received waveform consists of the received signal described previously and additive noise. This bandpass Gaussian noise is modeled as white over the received bandwidth.

In (2), it is assumed that the axial target size is constrained such that $0 < (2z/c) < T$ for all z. Therefore, the received signal during any interval represents the return from the pulse launched during the same interval. Simplifications of the model in (2) are presented in Appendix A. These simplified models are used in the derivation of the maximum likelihood estimators.

III. Statistics of the Received Signal

The evaluation of the statistics of the received signal is important for two reasons. First, the total received signal can be modeled as a Gaussian random process and is therefore completely specified by its mean and autocovariance. In this case, the effect of the scatterer velocity on the statistics of the received signal can be determined analytically. It will be shown that the mean velocity and the presence of multiple velocity components affect the envelope and phase of the autocovariance. Second, in order to derive the maximum likelihood estimator for the velocity, which is carried out in the next section, the autocovariance of the received signal must be evaluated.

In order to evaluate the mean and autocovariance of the random process, we must make some assumptions on the statistical models. We assume that the scatterers are identically distributed and that the lateral beam weighting is approximately zero at a radius R'. We also assume that the distribution of z_i is uniform over $[c \cdot d'/2 - M, c \cdot d'/2 + M]$, where M is a distance which is much larger than the axial sample volume size. The term $\exp[j\sigma z_i]$ in (2) thus represents a random phase that is uniformly distributed over $[0, 2\pi]$. The process is obviously nonstationary. It is easily shown that the $\mathcal{E}[r'(t)] = 0$ because of the uniform distribution of the phase.

The statistics of $r'(t)$ can then be completely specified by the autocorrelation. The derivation of the autocorrelation follows the theory developed in statistical physics and applied to ultrasound for narrowband signals by Atkinson [2] and by Mo and Cobbold [9]. The result, presented here, differs from [2] and [9] due to the use of a signal with significant fractional bandwidth and a model that includes the movement of the sample volume.

The result for the complex autocorrelation is a triple integral over the beam coordinates of the product of terms involving the lateral beam sensitivity, the Doppler shift, and the deterministic signal envelope. The expression for the autocorrelation is

$$R_r(t, u) = \sigma_a^2 \mathcal{W} \tilde{n} \pi E_t \int_{cd'/2-M}^{cd'/2+M} \int_0^{2\pi} \int_0^{R'} rb[r(t)]b[r(u)] \exp -\left[j\sigma v(\tilde{r})\cos\alpha(t - u)\right] \sum_i s'\left(t - 2z/c - kT[1 + 2v(\tilde{r})\cos\alpha/c]\right) \sum_i s'^*\left(u - 2z/c - lT[1 + 2v(\tilde{r} \cdot \cos\alpha/c]\right) dr\, d\Phi\, dz. \quad (3)$$

The first term, σ_a^2, represents the variance of the scatterer amplitude. The quantity $\mathcal{W}$ is called the packing factor and is a measure of the correlation among scatterers. This quantity and therefore the power in the received signal approach zero for a uniformly dense medium at a very high volume concentration. The notation $\tilde{n}$ indicates the average scatterer concentration

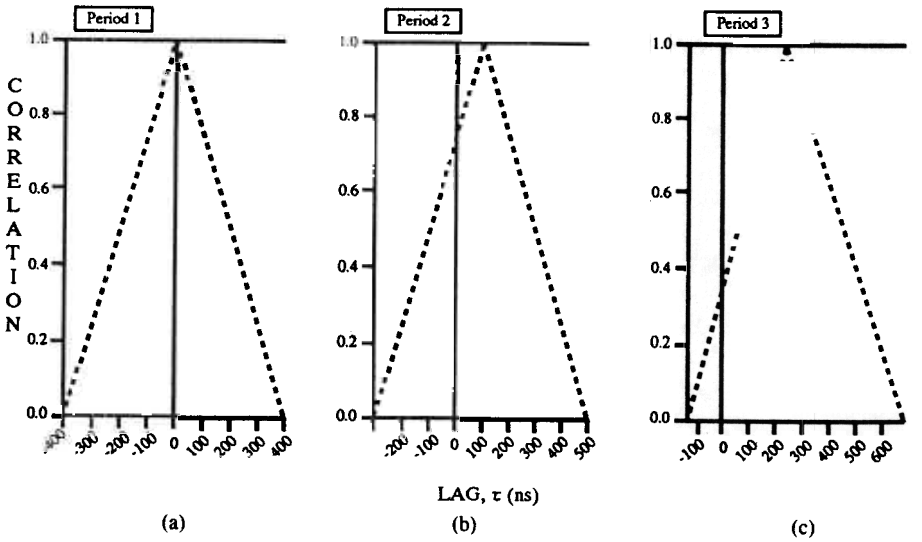

Fig. 2. Normalized magnitude of the autocorrelation of the received signal from uniform velocity scatterers using a long periodic pulse train with transmitted period T as a function of lag (ns). (a) Autocorrelation for $-400 < t - u < 400$ ns. (b) Autocorrelation of the received signal, the zero lag axis shows $t - u = T$. (c) Autocorrelation of the received signal, the zero lag axis shows $t - u = 2T$.

within a unit volume [2], [9]. Note that it has been postulated that these quantities change in the presence of turbulence and may therefore represent a measure of turbulence. Due to the transmission of a wideband signal, the potential exists to evaluate these parameters for small spatial volumes and thus map any change in their magnitude across the vessel.

The term $b[r(t)]b[r(u)]$ represents the variation in lateral beam sensitivity with the position of the scatterer. The next term in the autocorrelation represents the Doppler shift. The sum over k or l represents the sum over the individual pulses or periods. The deterministic received pulse s' is delayed according to the location of the moving scatterers. Therefore the received period, given by $T[1 + 2v(\bar{r}) \cos \alpha/c]$, changes due to the velocity of the scatterers.

The peak of the magnitude of the correlation can be used to estimate the velocity of the scatterers. We show this by letting $m = k - l$ and $\tau = t - u - mT$. Evaluating (3) for a uniform velocity v, the integral of the received envelopes over z then results in a waveform whose peak occurs at the lag value $\tau = mT[2v/c]$.

A. Numerical Evaluation of the Autocorrelation

The goal of this section is to develop insight into the effect of the mean scatterer velocity and the presence of a velocity spread target on the magnitude of the autocorrelation of the received signal. The effect of the velocity distribution on the mean and autocorrelation is compared with the computed statistics from acoustic data in Part II of this paper [19]. It will be shown that this relatively simple model that neglects turbulent flow, accurately predicts the changes in the autocorrelation due to the illuminated velocity distribution. The autocorrelation is evaluated for two physical situations, a uniform velocity nonfluctuating target and a velocity spread target.

The magnitude of the correlation is evaluated for the following parameters: the center frequency, f_o, is 5 MHz, and the envelope of the received signal, denoted $s'(t)$, is real and rectangular and of 400 ns duration, with a pulse repetition period, T, of 10^{-4} s. The lateral sensitivity of the sample volume is Gaussian and centered within the vessel, using a beam-vessel angle of zero degrees. In this evaluation, a constant number of pulses overlap for values of $t - u < 3T$ due to the assumption that P pulses are transmitted and N pulses are used in the evaluation of the correlation, such that $P - N > 2$.

The numerical evaluation of (3) using a uniform scatterer velocity of 1 m/s is shown in Fig. 2. In Fig. 2, the autocorrelation consists of a series of *periodic* triangular functions *centered at the integer multiples of* $T[1 + 2v/c]$, where v is the scatterer velocity. In this case, the scatterer velocity of 1 m/s produces a shift in the peak of the correlation of 130 ns.

Although not shown, the phase of the correlation is constant for each period due to the uniform scatterer velocity. Therefore, *both* the period of the autocorrelation and its phase contain information concerning the velocity, v, of the scattering medium.

As shown in Fig. 2, the magnitude of the autocorrelation at multiples of T is reduced by the effect of scatterers leaving the sample volume. This demonstrates the need to "track" the scattering medium when the transmitted signal is wideband, because in such a case the autocorrelation decreases rapidly as a function of the number of transmitted periods. In Fig. 2, the correlation at $t - u = 2T$ is approximately equal to 0.38. This is a result of the "transit time effect," or the effect of scatterers leaving the sample volume. The resolution of purely frequency based procedures would therefore be extremely limited, using this wideband transmitted signal. This again emphasizes the spatial-velocity resolution tradeoff inherent in narrowband "Doppler" estimation.

For comparison, Fig. 3 shows the numerical evaluation of (3) using a laminar parabolic velocity profile with a peak velocity of 1 m/s, and an ultrasonic beam width with a standard deviation of 42.5% of the radius of the vessel. The peak of the correlation occurs at multiples of (T + 120 ns), corresponding to a velocity of 0.92 m/s.

The magnitude of the correlation peak and the integral of the correlation decrease rapidly as a function of the lag index m, upon illumination of this velocity spread target. The periodicity

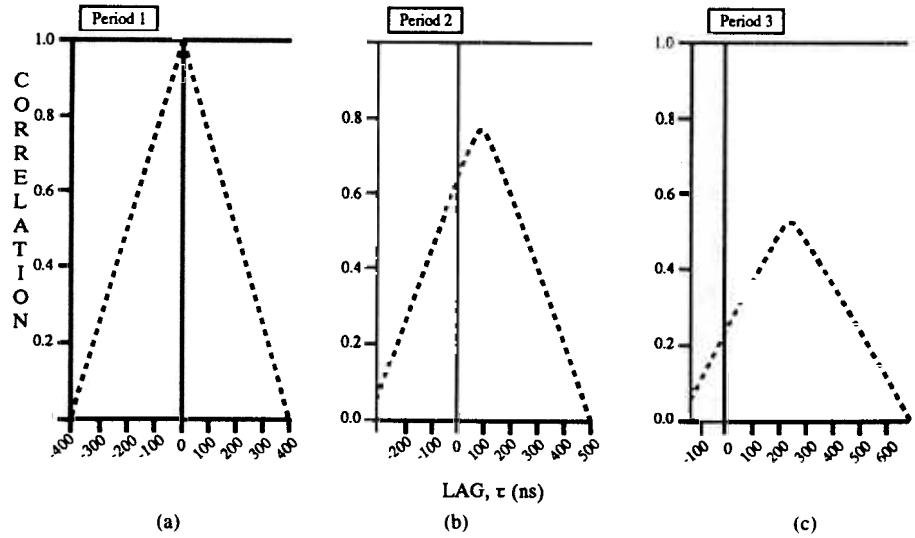

Fig. 3. Normalized magnitude of the autocorrelation of the received signal from a velocity spread target using a long periodic pulse train with transmitted period T as a function of lag (ns). (a) Autocorrelation for $-400 < t - u < 400$ ns. (b) Autocorrelation of the received signal, the zero lag axis shows $t - u = T$. (c) Autocorrelation of the received signal, the zero lag axis shows $t - u = 2T$.

of the magnitude of the autocorrelation is destroyed, and this destruction depends only on the spread of the illuminated velocity distribution. Since the magnitude of the autocorrelation decreases with m, the maximum lag for which a significant correlation exists also decreases. Therefore, the heuristically optimum estimation strategy would illuminate a small region (with a narrow velocity distribution) and utilize a smaller number of transmitted periods in the presence of a velocity spread target.

B. Discussion of Section III

The following conclusions can be drawn from (3) and are illustrated by the numerical evaluation of the autocorrelation. The *location of the peak of subsequent periods* of the autocorrelation is shifted by the target velocity. The scatterer velocity can be predicted from the period of the peak of the autocorrelation. In addition, the magnitude of the peak and the shape of the autocorrelation are strongly affected by the presence of a velocity spread target within the sample volume.

Although not shown, a nonzero beam vessel angle also limits the length of the correlated signal received from a group of scatterers. For a target with a uniform velocity, this limit, which results from the transit time of the scatterers has previously been evaluated [2], [4], [11].

This study of the autocorrelation illustrates that there is information concerning scatterer velocity in the magnitude and phase of the correlation of the received signal. We consider now the optimal processing of this information to determine mean scatterer velocity and the velocity distribution.

IV. Maximum Likelihood Velocity Estimation

Following a brief discussion of target estimation theory, the wideband point MLE of the target velocity and the more complex wideband range spread MLE are derived. Since the sample volume may contain a velocity spread target, a mean velocity and velocity spread estimator are discussed.

The likelihood function $l(v)$ is given by Van Trees [12] for a general target as

$$l(v) = /N_o \int \int_{T_i}^{T_f} r'^*(t)h'(\qquad) r'(u)\, dt\, du \quad (4)$$

where T_i and T_f are the initial and final temporal limits imposed by a finite data window. The time varying filter $h'(t, u; v)$ is the solution of the integral equation

$$N_o h'(t, u; v) + \int_{T_i}^{T_f} h'(t, g; v) R_r(g, u)\, dg = R_r(t, u). \quad (5)$$

This equation cannot be solved in general without specification of the transmitted signal and specific assumptions concerning the velocity distribution of the scattering medium within the sample volume.

Previous Application of Wideband Estimation to Ultrasound and Radar: The MLE derived by Olinger [13] for ultrasonic applications used a general wideband signal and considered the entire temporal axis of the received waveform to be scaled by velocity. Olinger also included lateral beam modulation within his derivation, but excluded the range spread or velocity spread nature of the target.

A velocity estimation structure for radar applications which utilized the change in position and frequency was also discussed by Helstrom [14]. Helstrom considered joint maximization of both delay and velocity. In our case we consider only the maximum likelihood over all possible velocities *for an assumed initial position.* Other studies of wideband maximum likelihood estimation for radar systems followed Helstrom's work. Kelly [15] and Rihaczek [16], [17] again considered the joint MLE of velocity and range, in the case in which range, velocity, acceleration, and higher order derivatives must all be estimated. Again the processors and their performance in our case are different, because maximization is carried out only over the velocity parameter.

The Effect of the Velocity Spread Target on the MLE: Due to the transmission of a wideband signal, the size of the sample

volume and therefore the range of velocity components present is reduced. If the spread of velocity components within a spatial volume is much less than the resolution of the estimator, the target is considered to be underspread, and the maximum likelihood estimate of velocity is given by the maximum of $l(v)$ using the wideband point MLE or the wideband range spread MLE. Otherwise, since the spatial mapping of the velocity within the small sample volume cannot be exactly determined, parameters of the velocity distribution within this volume are estimated. The velocity distribution and its moments are estimated from the likelihood function evaluated at a discrete set of velocity values.

In Section III, the length of the correlated signal from a velocity spread target was shown to be limited, thus constraining the time interval available for each estimate. In addition, since the target velocity also varies in the axial dimension, and the sample volume moves with the period index, a limit must be placed upon the number of pulses or periods used in each estimate. The resulting time interval is referred to as the data window.

Forms of the MLE: The MLE for the slowly fluctuating point target (SFPT) model discussed in Appendix A is considered due to the simplicity of the resulting estimator. The MLE for a range spread target is then proposed, and the performance of the two estimators is compared in the following sections.

A. Wideband Point MLE

Using the SFPT model, the maximum likelihood estimate of the axial velocity of the illuminated scatterers, denoted $\hat{v}$, is the $\max_v l(v)$, where the likelihood is derived in Appendix B and given by

$$l(v) = \left| \sum_k \int_{-\infty}^{\infty} r'(t)\, s'^*(t - d - kT[1 + 2v/c]) \cdot \exp[j\sigma v t]\, dt \right|^2. \quad (6)$$

The data window is implemented by placing a finite limit on the summation over the index k, thus limiting the number of periods used in an estimate.

The estimator is an explicit function of velocity in the *period* of the returned signal and the center frequency of the complex envelope. Equation (6) can be rewritten in the following classical form.

$$l(v) = \int \int_{-\infty} r'^*(t) h'(t, u; v)\, r'(u)\, dt\, du \quad (7)$$

where

$$h'(t, u; v) = \sum \sum s'(t - d - kT[\ \ + 2v/c]) \cdot \exp[-j\sigma v t]\, s'^*(u - d - lT[1 + 2v/c]) \cdot \exp[j\sigma v u] \quad (8)$$

It is the factorization of (7) into the magnitude squared form of (6) that simplifies the implementation of this estimator. A single sum over the index k is required in (6), reducing the computational requirements of this estimator.

This receiver may be implemented using a correlation receiver, or matched filter. Using the correlation receiver, a train of pulses whose delay *and* center frequency are varied for each velocity component is multiplied by the received signal. Using the matched filter approach, two options are available. The impulse response of the filter may again consist of a train of pulses whose delay *and* center frequency are varied for each velocity component. A physically simpler approach would utilize a set of delay lines which delay the received signal from each pulse by $(P - k)T[1 + 2v/c]$, where k is the period index and P is the total number of periods used in the estimate. The output of these delay lines is followed by a simpler filter matched to the pulse envelope and center frequency. The implementation of this estimator is shown in Fig. 4.

Finally, we note that the estimator matches the returned signal with the complex envelope $s'(t)$, where $s'(t)$ represents the filtered transmitted signal. The filter incorporates the effect of frequency dependent attenuation, and the frequency dependence of the scattering function. If an estimate of the tissue type and depth can be made, the MLE could be adapted to reduce these effects.

B. Wideband Range Spread Maximum Likelihood Estimator

Consideration of the range spread nature of the target is now included in the derivation of the maximum likelihood estimator. The wideband range spread MLE is derived in Appendix C and the likelihood, $l(v)$, which is then maximized over v is defined in (9) and (10):

$$l(v) = /N_o \int \int_{T_i}^{T_f} r'^*(t) a(t) h'(t - u; v) w_1(t - u) r'(u) a(u)\, dt\, du \quad (9)$$

$$h'(t - u; v) = \mathfrak{F}^{-1}\left[\frac{\mathfrak{F}\left\{ E_r \sum_g w_2(g) R_s(t - u - gT[1 + 2v/c]) \exp[-j\sigma v(t - u)] \right\}}{N_o + \mathfrak{F}\left\{ E_r \sum_g w_2(g) R_s(t - u - gT[1 + 2v/c]) \exp[-j\sigma v(t - u)] \right\}} \right] \quad (10)$$

where the notation $R_s[t - u - gT(1 + 2v/c)]$, using $g = (k - l)$, describes the effect of the range spread target on the deterministic signal s', and is defined by

$$R_s[t - u - gT(\ \ + 2v/c)] = \int_{cd'/2 - M}^{cd'/2 + M} s'[t - 2z/c - kT(1 + 2v/c)]\, s'^*[u - 2z/c - lT(1 + 2v/c)]\, dz \quad (11)$$

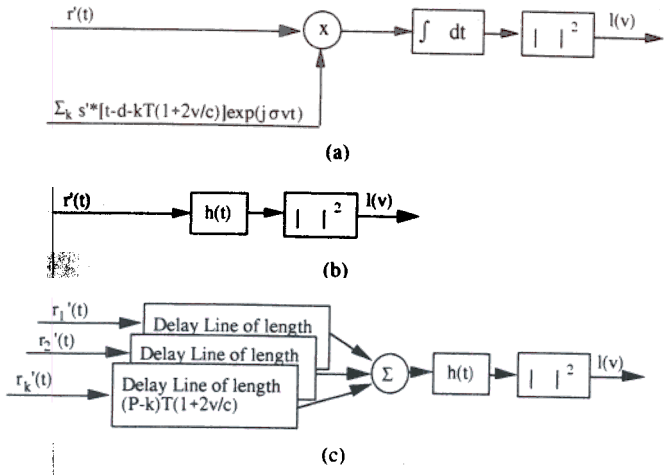

Fig. 4. Implementation of the wideband point MLE. (a) Correlation receiver. (b) Matched filter, matched to $\Sigma_k s'^*(t - d - kT[1 + 2v/c]) \exp[j\sigma v t]$. (c) Bank of delay lines, and filter matched to $s'^*(t) \exp[j\sigma v t]$. Simplified matched filter using P pulses for an estimate, where $r_k'(t)$ is the return from the kth pulse.

The novel aspects of the receiver are contained in the filter $h'(t - u; v)$. For each velocity, v, the filter has a center frequency of σv, and a frequency envelope determined by the Fourier transform of $R_s[t - u - gT(1 + 2v/c)]$. This frequency envelope is multiplied by a train of frequency pulses with a period of $2\pi/\{T[1 + 2v/c]\}$. Again, both the Doppler frequency shift and the period are determined by the velocity, v. Note that the estimator cannot be factored into a magnitude squared form, and therefore this estimator requires P^2 computations, where P is the number of periods or pulses used in the estimate. The implementation of this estimator is shown in Fig. 5.

Although this estimator is derived based on the range spread target model presented in Appendix A, the presence of axial velocity variations in the true target necessitates the estimation of the scatterer velocity at discrete points in range. This requires the imposition of a temporal window along each vector, which is referred to as the axial window, $a(t)$. In addition, for the range spread MLE the data window is implemented using finite limits of integration and the window $w_1(g)$.

C. Estimation of Mean Velocity

Since the velocity spread of the received signal may exceed the resolution of the estimator, we consider estimation of the mean velocity. In this receiver structure, the likelihood is evaluated for discrete axial velocity components v_j, and the mean velocity receiver implements the ratio of the first moment of the likelihood function divided by the zeroth moment. The estimate of the mean velocity is defined by

$$\hat{v}_m = \sum_j v_j l(v_j) \Big/ \left[\sum_j l(v_j) \right]. \tag{12}$$

The mean velocity receiver can be implemented using the wideband point or range spread structure with the appropriate filters used in each parallel path.

D. Estimation of Velocity Spread

Although a detailed discussion of velocity spread estimation is beyond the scope of this paper, the basic concept is presented. It is shown in [10] that the width of the $l(v)$ in the v dimension increases for a velocity spread target. The second moment of the likelihood can therefore be used as an estimate of the velocity spread of the target. In addition, from the results of Section III we note that the correlation magnitude for each t and u, and the correlation integrated over all values of t and u, decrease when the illuminated volume contains a velocity spread target.

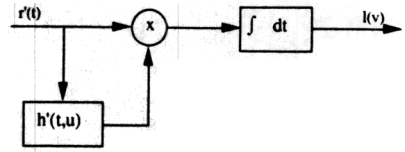

Fig. 5. Implementation of the wideband range spread MLE using a matched filter.

For the wideband point MLE, the expected value of $l(v)$ is given by

$$\mathcal{E}[l(v)] = \int \int_{-\infty} \mathcal{E}[r'^*(t) r'(u)] h'(t, u; v)\, dt\, du. \tag{13}$$

Therefore, using (13), it can be shown that the peak magnitude of the expected likelihood function also decreases under these conditions. The maximum magnitude of the wideband MLE for each spatial location can thus be used to estimate the illumination velocity spread.

Summary: New maximum likelihood estimators for the velocity of blood scatterers have been obtained for wideband periodic transmitted signals using a point and range spread target model. The local and global accuracy of these estimators are now evaluated using the statistical signal model.

V. Local Accuracy

The local accuracy of the wideband point MLE and wideband range spread MLE is studied by considering the bounds on their variance. The SFPT model discussed in Appendix A is used to facilitate a comparison to other estimation strategies. The bound on the variance of the wideband MLE is then evaluated for a range spread target. In the presence of a range spread target, the variance of the wideband point MLE will be shown to increase, and the wideband range spread MLE shown to decrease the variance in such a case. In each case the expressions presented were derived in the absence of frequency dependent attenuation.

Local Accuracy and the Cramer–Rao Bound: The estimator's local accuracy is evaluated under the assumptions that the energy to noise ratio is large, and the errors are small. The Cramer–Rao bound provides a lower bound on the accuracy of any unbiased estimate. For a general estimator, or a general target the Cramer–Rao bound becomes

$$\operatorname{var}[\hat{v} - v] \geq \Big[-1/N_o \int \int_{-\infty}^{\infty} \partial R_r(t, u)/\partial v' \, \partial h'(t, u; v)/\partial v \, dt\, du \Big]^{-1}_{v = v'} \tag{14}$$

The Cramer–Rao bound is proportional to the second derivative of the ambiguity function. The ambiguity function for a slowly fluctuating point target is the expected response, in the absence of noise, of the likelihood receiver, due to a point source at some fixed point in the range velocity space. The expectation is taken over the entire range velocity space. In Section VI the expected estimator output or ambiguity function is

computed and plotted. The first and second derivative of the ambiguity function can then be observed and compared to the bound.

A. Variance of the Wideband Point MLE with a SFPT

The expression for the bound on the variance of a wideband point ML estimate of the axial velocity in the presence of a slowly fluctuating point target and in the absence of frequency dependent attenuation is derived in Appendix D and is given by

$$\operatorname{var}[\hat{v} - v] \geq \left[8/c^2(E_r/N_o)\left\{w_o^2[\mathcal{E}(t^2) - \mathcal{E}(t)^2] + [\mathcal{E}(w^2) - \mathcal{E}(w)^2]\right\}\right]^{-1} \quad (15)$$

where the expectations in the denominator of (15) are given by

$$\mathcal{E}[w^2] = \sum (kT)^2 P \int_{-\infty}^{\infty} s'^*(u - d - kT - \phi_k v) \partial^2/\partial(\phi_k v)^2 [s'(u - d - kT - \phi_k v)]\, du \quad (16)$$

$$\mathcal{E}[w = \left| \sum_k kT \int_{-\infty}^{\infty} \partial/\partial(\phi_k v) s'^*(u - d - kT - \phi_k v\, s'(u - d - kT - \phi_k v)\, du \right| \quad 17$$

$$\mathcal{E}[t^2] = P \int_{-\infty}^{\infty} \sum_k u^2 \left| s'(u - d - kT - \phi_k v) \right|^2 du \quad 18)$$

$$\mathcal{E}[t]^2 = \left[\int_{-\infty}^{\infty} \sum_k t \left| \quad (t - d \cdot kT - \phi \quad) \right|^2 dt \right]^2. \quad (19)$$

The denominator of (15) contains the sum of two terms. The first term, $w_o^2[\mathcal{E}(t^2) - \mathcal{E}(t)^2]$, results from the phase information in the received signal, and the second term, $\mathcal{E}(w^2) - \mathcal{E}(w)^2$, results from estimation of the delay of the received signal. We now consider the choice of conditions which minimize the bound in (15). Maximization of the first term in the denominator of (15) requires maximization of the $\mathcal{E}[t^2]$. Due to the use of the SFPT model, the effect of the transit time of the scatterers through the lateral beam, or of a velocity spread target within the sample volume is not explicitly shown in (18). It is shown in [10] that these factors limit the length of the coherent signal from a group of scatterers, and therefore determine the maximum value of the $\mathcal{E}[t^2]$. The variance bound is therefore minimized by the choice of a data window (determined by the number of periods used per estimate) that maximizes the $\mathcal{E}[t^2]$. Using the wideband MLE strategy, that data window can equal the length of the coherent signal *from each group of scatterers*. Extending the data window beyond the coherent signal length would decrease the signal to noise ratio without improving the performance of the estimator. This suggests that additional estimates which can then be made using subsequent data windows should be averaged using a total duration that is less than the period of stationarity of the cardiac dynamics. Therefore, the selection of the optimal data window for a group of scatterers is critical to the quality of the estimate. From term one in the denominator of (15), we also observe that the variance can be decreased by an increase in the center frequency of transmission.

As for term two, which results from the use of the signal delay, it is proportional to the squared bandwidth of the signal, normalized within (16) by a measure of the squared coherent signal duration. This coherent signal duration is again maximized by a data window that is equal to the length of the coherent returned signal. Term two is significant only for a returned signal of substantial fractional bandwidth, and increases with the fractional bandwidth of the returned signal.

It is also important to note the presence of P (the number of periods) in (16) and (18). For an even signal with a symmetrical bandwidth, P combined with the signal to noise ratio (E_r/N_o), where E_r represents the received power from a single pulse, clearly shows the signal to noise improvement that results from the use of P pulses or periods in each estimate.

Finally, we note that for a data window that is less than the transit time of the scatterers through the lateral beam, the variance of the wideband point MLE calculated from (15)–(19) is unchanged by the magnitude of the velocity of the scatterer.

Comparison to the Narrowband MLE (NMLE): The narrowband MLE for a slowly fluctuating point target is a classical structure derived by Van Trees [12]. For maximization over velocity space and using a wideband transmitted signal, the bound on the variance is given by

$$\operatorname{var}[\hat{v} - v] \geq \left\{8/c^2(E_r/N_o)w_0^2(\mathcal{E}[t^2] - \mathcal{E}[t]^2)\right\}^{-1} \quad (20)$$

where

$$\mathcal{E}[t^2] = \int_{-\infty}^{\infty} \sum_k u^2 s'(u - d - kT) \cdot s'^*(u - d - kT[1 + 2v/c])\, du \quad (21)$$

where P' is the number of received pulses for which the integral of the product $s'^*(u - d - kT\, s'^*(u - d - kT[1 + 2v/c])$ is significant.

The denominator of the bound on the variance of the narrowband MLE (20) again results from the phase information in the received signal. Using a wideband transmitted signal and the NMLE, the maximum value of $\mathcal{E}[t^2]$ in (21) is clearly limited by the axial signal length $s'(\cdot)$, since the product of $s'(u - d - kT)s'^*(u - d - kT[1 + 2v/c])$ equals zero after a number of periods which depends on the scatterer's velocity. The value of $\mathcal{E}[t^2]$ in (21) is therefore significantly decreased by the stationary sample volume, and the bound on the variance is much larger. In order to achieve comparable performance with the narrowband estimator, $s'(\ )$ must be lengthened and thus a narrowband signal must be transmitted, thereby degrading spatial resolution.

The value of $\mathcal{E}[t^2]$ in (21) also clearly depends on the magnitude of the velocity of the scatterer. Therefore the axial signal length required to maximize $\mathcal{E}[t^2]$ depends on the velocity of the scatterer and cannot be maximized for all regions of scatterers. In addition, using a wideband transmitted signal and the NMLE, the variance of the narrowband estimator increases as the velocity of the scatterer increases.

Using (15) and (20), the standard deviation of the narrowband and wideband point maximum likelihood estimators is plotted versus scatterer velocity in Fig. 6, for a transmitted pulse train consisting of 16 pulses, with a center frequency of 5 MHz, a 50% fractional bandwidth, a pulse repetition period of 100 us and E_r/N_o equal to 1.

Generalized Comparison: It is shown in this section that (15) unifies previous results for Doppler frequency estimation and time shift correlation. As discussed above, the first term in denominator of (15) results from the effect of velocity on the frequency of the returned signal and corresponds to the denominator of (20). The second term is proportional to the squared bandwidth of the signal, normalized within (16) by a measure of the squared signal duration, and results from the

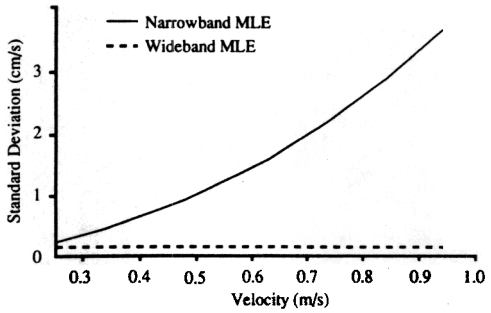

Fig. 6. Standard deviation of the wideband point MLE and narrowband MLE as a function of the velocity of the scatterers.

effect of scatterer velocity upon the delay of the returned signal. It can be shown, [10], that this second term has the same general form as the denominator of the velocity variance using the time shift correlation technique. In time shift correlation, two pulses are used in the generation of a single estimate, and thus the $\mathcal{E}[w^2]$ equals the product of the squared bandwidth and squared pulse repetition period, and the variance of the velocity estimate is inversely proportional to $\{E_r/N_o[\mathcal{E}(w^2) - \mathcal{E}(w)^2]\}$ [7], [10]. The use of two pulses in the generation of a single cross correlation estimate significantly reduces the $\mathcal{E}[w^2]$, as defined in (16), and therefore increases the variance in comparison with the wideband MLE for a fixed SNR. On the other hand, increasing the period T increases the $\mathcal{E}[w^2]$, but also decreases the pulse to pulse correlation, and thus increases the variance of the cross correlation estimate [7]. Although averaging successive cross correlation estimates reduces the variance, the resulting variance is larger than the bound on the wideband point MLE, for which an even pulse train is inversely proportional to the $\Sigma_l (lT)^2$, as shown by (15)–(19).

From the discussion above, it follows that in the absence of significant frequency distortion, the bound on the variance of the wideband MLE is smaller than the variance of an estimator which only uses phase or delay information. This is due to use of the maximum data window, which can be optimized for each axial region producing the coherent summation of the maximum number of periods, and to the sum of the two terms in the denominator of (15).

B. Variance of the Wideband Point MLE with a Range Spread Target

The degradation in performance of the wideband point MLE in the presence of a range spread target, is now evaluated using the range spread target model discussed in Appendix A. The bound on the variance for a real envelope is again given by (15), although the form of the expectations has changed [10]. The effect of the range spread target on $\mathcal{E}[w^2]$ and $\mathcal{E}[t^2]$ represent the major change in the bound. For the range spread target these terms are defined by,

$$\mathcal{E}[w^2] = \int_{cd/2-M}^{cd/2+M} \int_{-\infty}^{\infty} \sum_l (lT)^2 \cdot \partial/\partial(\phi_l v)\,[s'^*(u - d - lT - \phi_l v)] \cdot \partial/\partial(\phi_l v)\, s'(u - 2z/c - lT - \phi_l v)\, du \int_{-\infty}^{\infty} \sum_k s'(t - d - kT - \phi_k v \cdot (t - 2z/c - kT - \phi_k v)\, dt\, dz \qquad (22)$$

$$\mathcal{E}[t^2] = \int \int \sum \sum u^2 s'^*(u - d - lT - \phi_l v)\, s'^*(t - d - kT - \phi_k v) \int_{cd/2-M}^{M} s'(u - 2z/c - lT - \phi_l v \cdot s'(t - 2z/c - kT - \phi_k v)\, dz\, du\, dt. \qquad (23)$$

The $\mathcal{E}[w^2]$ no longer simply represents the normalized squared bandwidth of the signal. Instead it represents the normalized squared bandwidth of the signal s convolved with itself. The value of the $\mathcal{E}[w^2]$ is therefore clearly decreased by the range spread target, and the variance is increased.

The effect of the spread target upon the $\mathcal{E}[t^2]$, (23), depends upon the pulse train length and on the transit time through the lateral beam width. If the data window is much smaller than the transit time, the $\mathcal{E}[t^2]$ is unchanged by the spread target. If the data window is on the order of the transit time through the lateral beam width, the $\mathcal{E}[t^2]$ becomes an average transit time which considers the initial position of all scatterers passing through the lateral beam width.

Example: As an example, a wideband Gaussian signal is used in the evaluation of the bound on the variance using (15). With the signal amplitude properly normalized, we find that the $\mathcal{E}[w^2]$ for a range spread target, (23), is one half of the point target value, (15), and the bound on the variance of the wideband point MLE increases. Regardless of the target, the bound on the variance of the wideband point MLE remains smaller than the narrowband MLE bound, however. This is due to the significant difference in the $\mathcal{E}[t^2]$ possible when using a wideband transmitted signal.

C. Variance of the Wideband Range Spread MLE with a Range Spread Target

The wideband range spread MLE was defined by (9) and (10). The bound on the variance of this estimator for a single velocity component can be derived using (14) [10]. For a real, even received envelope, letting $\tau = t - u$, and

$$R'_s(v) = \sum E_r w_1(g) w_2(g) R_s(\tau - gT[1 + 2v/c]), \qquad (24)$$

$$R'_{s2}(v = \sum E_r w_2(g) R_s(\tau - gT + 2v/c])$$

The bound is given by,

$$\text{var}[\hat{v} - v] \geq \left\{ \int_{-\infty}^{\infty} 2E_r\sigma^2 \left[\mathfrak{F}\{\tau R'_s(v)\} \mathfrak{F}\{\tau R'^*_{s2}(v)\} \right] / \left(N_o + \mathfrak{F}\{R'_{s2}(v)\}\right)^2 dw + \int_{-\infty}^{\infty} 2E_r \left[\mathfrak{F}\{\partial R'_s(v \partial v\} \mathfrak{F}\{\partial R'^*_{s2}(v), \partial v\} \right] / \left(N_o + \mathfrak{F}\{R'_{s2}(v)\}\right)^2 dw$$

The first term represents the temporal spread of the autocorrelation, and is analogous to term one in the denominator of (15). Term two is a measure of the bandwidth of the filtered autocorrelation and is analogous to term two in (15). In each

term, the effect of the denominator is to increase the effective bandwidth and therefore decrease the variance.

Evaluation of the Variance of the Wideband Range Spread MLE for a Specific Transmitted Signal: Equation (26) has been evaluated for a four pulse transmitted signal with a Gaussian envelope of standard deviation $300/\sqrt{2}$ ns, with a pulse repetition period of 100 us, and a signal to noise ratio of 20 dB. The bound on the variance decreases by a factor of 1.8 in comparison with the wideband point MLE in the presence of a range spread target.

D. Variance of the Mean Velocity Estimate

The bound on the variance of the *mean velocity estimator*, which was described in (12), is now evaluated. Assuming that the contribution of the sum $\Sigma_j l(v_j)$ to the variance is negligible, [4], and assuming the bins to be independent, the bound on the variance of the mean velocity estimate can then be written as the weighted sum of individual components indexed by j.

$$\text{Var}\,[\hat{v}_m - v_m$$

$$\sum v \;\; \text{Var}\,[l(v_j)] \;\; \Big/ \Big[\sum_{\cdot} \mathcal{E}\{l(v_j)\} \qquad v_m^2 \qquad (27)$$

Each component has the form

$$\text{var}\,[l(v_j)] \geq \left[8/c^2(E_r/N_o)\left\{w_o^2[\mathcal{E}(t^2) - \mathcal{E}(t)^2] + [\mathcal{E}(w^2) - \mathcal{E}(w)^2]\right\}\right]^{-1}. \qquad (28)$$

From (27), we observe that the bound on the variance of the mean velocity estimator increases with the width of the velocity distribution, as was expected.

Summary: An expression for the bound on the variance of the wideband point MLE in the presence of a point target has been derived. This bound has been shown to be smaller than the variance of competing strategies, but increases in the presence of a range spread target. Using the wideband range spread MLE, the bound on the variance in the presence of a range spread target can be reduced further. Additional improvement can also be achieved by increasing the transmitted bandwidth or the center frequency of transmission. When the mean velocity is estimated, the bound on the variance also depends upon the spread of the velocity distribution of the target.

VI. Expected Output of the Estimator: Global Accuracy

In this section, the improvement in global accuracy due to the transmission of a signal with significant fractional bandwidth and a wideband estimation strategy is discussed. First, the classical theory of global accuracy for narrowband and wideband signals is reviewed. It will be shown that the use of the wideband MLE produces a reduction in the width of the mainlobe and in the height of velocity sidelobes. Next, the global accuracy of the wideband point MLE will be shown to be degraded in the presence of a range spread target. Finally, the performance improvement due to the wideband range spread MLE is evaluated.

Throughout this section β is used to differentiate the true axial scatterer velocity from the estimated axial velocity, v. Conclusions are presented based upon the appropriate ambiguity function. Examples are then presented to illustrate these conclusions. In the examples, unless otherwise stated, a two-cycle rectangular pulse envelope $s'(t)$ with a center frequency of 5 MHz and a pulse repetition period of 100 μs are assumed.

Global Accuracy of MLE: In order to consider the global accuracy, we remove the assumption that the errors are necessarily small. Since the transmitted signal is often a pulse train, the ambiguity function is assumed to have subsidiary peaks that are non-negligible. The method used by Van Trees [12] for evaluation of global accuracy is less useful in the presence of subsidiary peaks. As Van Trees states, the numerical results add little insight in the presence of multiple peaks. The approach taken in this paper is to evaluate the mainlobe and the height of the first subsidiary peak. The width of the mainlobe determines the velocity resolution. Because of the presence of aliasing, the subsidiary peak leads to a significant error, and therefore the height of this peak is discussed.

Classical Theory of Global Accuracy: Global accuracy is considered for the wideband MLE through a discussion of the generalized ambiguity function. The term "generalized ambiguity function" is intended to include wideband transmitted signals and other factors that cannot be described by the Woodward [18] or narrowband ambiguity function. In the absence of acceleration, or higher-order temporal derivatives, the generalized ambiguity function is defined [15] on the range velocity space by

$$q(r, x; r', x') = 1/2 \text{ Re}\left\{\exp\left[jw_o x(r \quad r)\right] Q(r, x; r', x')\right\} \qquad (29)$$

where

$$Q(r, x; r \qquad \int \; S^*[x(t + r' - r)]S[x'(t)] \cdot \exp\left[jw_o(x - x')t\right] dt. \qquad (30)$$

This is the response of the likelihood function matched to parameters r and x, due to a target with parameters r' and x', where $cr/2$ represents the target range at time $t = r/2$, $x = (1 - 2v/c)$ and is thus an indicator of target velocity, and $S(t)$ is the complex envelope of the transmitted signal. In the following we let $w' = w_o(x - x')$.

The "modulation function" Q is analogous to the Woodward ambiguity function. The function simplifies to the Woodward form if the velocity information in the complex envelope is ignored. For a periodic transmitted signal, the narrowband ambiguity function reaches a value near unity at integer multiples of $w' = 2\pi/T$ and produces a velocity ambiguity. For a periodic pulse train, it can be shown [15] that the transmission of a wideband signal reduces the amplitude of peaks at integer multiples of w' in the generalized ambiguity function due to the tracking of the complex envelope. *Thus for wideband transmitted signals the height of the subsidiary velocity peaks is significantly diminished.*

Spread Ambiguity Function: In the evaluation of the wideband range spread MLE, the spread ambiguity function is used which, as defined by Van Trees [12], is the expected output of the likelihood receiver in the absence of noise. For delay-velocity space *the spread ambiguity function* is calculated from

$$\theta(d, d', v, \beta) = \mathcal{E}[l(d, d', v, \beta)] \qquad (31)$$

$$l(d, d', v, \beta) = 1/N_o \int \int \quad r'^*(t)h'(t, u; v)\, r'(u)\, dt\, du$$

where d and v are the delay and axial velocity of the receiver, and d' and β are the average delay and the axial velocity of the *spread* target. In Sections VI-B and VI-C the spread target ambiguity function is evaluated for a fixed value of d that corresponds to a known location in the center of a spread target ($d = d'$), and plotted for all values of target velocity in a two dimensional plot of velocity versus likelihood. The expectation requires integration over the axial dimension.

A. Expected Output of the Wideband Point MLE with a SFPT Target

We first consider the expected estimator output of the wideband point MLE, which is evaluated in the presence of a *point* target, located at the axial position z. It will be shown in Section VI-B that the expected output of the wideband point MLE in the presence of a range spread target is equivalent to the spatial integral of the point target results presented in this section. Therefore the examples presented in this section can be used to predict the response of the estimator to targets initially located at particular axial positions. Using the SFPT model in Appendix A, and due to the small magnitude of the velocity component, this expression can be approximated as

$$\mathcal{E}\{l(v)\} \approx E_r \Big| \sum_k \exp\left(j\omega kT[v-\beta]\right) \int_{-\infty}^{\infty} s'^*[t - d - kT(\quad + 2v/c)] \cdot s'[t - 2z/c - kT(1 + 2\beta/c)]\, dt \Big|^2. \quad (33)$$

where d indicates the two way travel time of the signal, and z is the axial position of the *point* target.

The expression is the *generalized ambiguity function* described in (29) and (30) and *therefore has reduced subsidiary velocity peaks upon transmission of a wideband periodic signal.* In addition, since the second derivative of the ambiguity function near $v = \beta$ is inversely proportional to the Cramer–Rao bound, conclusions can be drawn regarding the local behavior of the ambiguity function. It was shown in Section V that the bound on the variance of the WMLE was inversely proportional to the data window, the transmitted signal bandwidth, and transmitted center frequency. In addition, the bound was shown to be independent of the velocity of the scatterer for a data window that is smaller than the length of the coherent signal. The local behavior of the ambiguity function therefore shares these properties.

Height of Subsidiary Velocity Peaks: In order to study the height of the first subsidiary peak at a delay that corresponds to the target location, we rewrite the expression for $\mathcal{E}\{l(v)\}$ letting $d = 2z/c$:

$$\mathcal{E}\{l(v)\} = E_r \Big| \sum_k \exp\left(-j\omega kT[v-\beta]\right) \cdot R_s[2kT(v-\beta)/c] \Big|^2 \quad (34)$$

where R_s is defined by (11). The maximum clearly occurs when $v = \beta$. Since $\Sigma_k R_s[2kT(v-\beta)/c]$ is a monotonic function of $v - \beta$, additional peaks occur when $\exp[jT\sigma(v-\beta)] \approx \exp[j2\pi m]$ or velocities slightly less than $\{\beta + 2\pi mc/(2w_oT)\}$, where m is a nonnegative integer which is used as the index of subsidiary peaks. The expected output is then given by

$$\mathcal{E}\{l(v)\}\Big|_{v=\beta+2\pi mc/(2w_oT)} = E_r \Big| \sum_k R_s(2\pi km/w_o) \Big|^2. \quad (35)$$

Since the width of R_s decreases with an increase in the signal bandwidth, (35) shows that the height of the subsidiary peaks decreases with an increase in the signal bandwidth. In addition, the expected estimator output in (35) clearly decreases as the index of subsidiary peaks, m, is increased. As an illustrative example, we evaluate (33) for a train of four Gaussian pulses and find that the ratio of the first subsidiary peak to the main peak equals 0.349 and 0.197 for Gaussian standard deviations of $300/\sqrt{2}$ and $200/\sqrt{2}$ ns respectively. Using eight pulses, the ratio decreases to 0.090 and 0.049 for the standard deviations of $300/\sqrt{2}$ and $200/\sqrt{2}$ ns. For an acoustic velocity of 1540 m/s and a standard deviation of $300/\sqrt{2}$ ns, the first subsidiary peak occurs at velocity 1.51 m/s, near the approximate peak of 1.54 m/s predicted from $v = \{\beta + 2\pi mc/(2w_oT)\}$.

The conclusions drawn from (33)–(35) are now illustrated through examples. Equation (33) was evaluated in Figs. 7 and 8 for a scatterer moving at 1 m/s, with d equal to zero, and using the rectangular transmitted pulse train discussed in the introduction to this section. The expected value was evaluated and plotted in three dimensions as a function of the axial position z and axial velocity v in Fig. 7, using four transmitted pulses, and Fig. 8, using eight pulses. Figs. 7 and 8 demonstrate that the slope of the $\mathcal{E}\{l(v)\}$ near $v = \beta$ clearly increases dramatically with the total number of pulses used in an estimate of the velocity of the scatterer. In addition, the width of the mainlobe clearly decreases with an increase in the data window. The performance of the wideband point MLE is independent of scatterer velocity for a data window that is less than the length of the coherent signal returning from a group of scatterers. The local and global accuracy would be identical for a scatterer velocity of 0 or 1 m/s.

Figs. 7 and 8 also illustrate the reduced height of the first subsidiary peak as compared to the central peak. The actual height is dependent upon the data window. As the number of pulses is increased from four to eight in Fig. 8, the height of the subsidiary peak decreases dramatically. Regardless of the data window, the smaller subsidiary peaks represent a significant improvement over narrowband or fixed sample volume strategies.

Narrowband Estimator or Stationary Sample Volume: For a narrowband receiver, point target, and wideband transmitted waveform the expected likelihood is given by

$$\mathcal{E}\{l(v)\} = E_r \Big| \sum_k \int_{-\infty}^{\infty} s'[t - 2z/c - kT(1 + 2\beta/c)] \, s'^*[t - d - kT] \exp\left[j\omega t(v-\beta)\right] dt \Big|^2.$$

Equation (36) shows that the narrowband receiver structure is mismatched to the wideband transmitted waveform due to the shift in the complex envelope s'. The presence of the scatterer velocity in the delay of the complex envelope causes the integral to decrease sharply as a function of the period index k. It can easily be shown that the mainlobe of the likelihood is therefore significantly increased. The performance of the narrow-

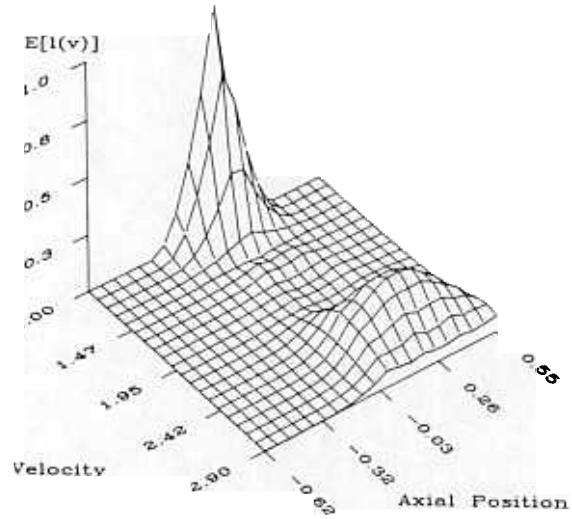

Fig. 7. Expected wideband point MLE output, using four transmitted pulses. Velocity, v, shown in m/s and axial position, z, in mm.

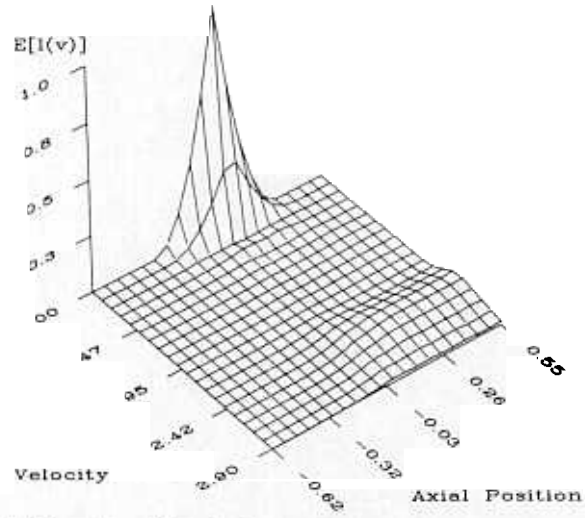

Fig. 8. Expected wideband point MLE output, using eight transmitted pulses. Velocity, v, shown in m/s and axial position, z, in mm.

band estimation structure can be improved only slightly by increasing the data window, since the scatterer quickly leaves the sample volume. In addition, the narrowband receiver performance varies significantly with the scatterer velocity.

Evaluating (36) for subsidiary velocity peaks where $v = \beta + 2\pi mc/(2w_o T)$, shows that the expected output is independent of m, and therefore the height of these peaks is approximately equal to the main peak.

Fig. 9 shows a three-dimensional (3-D) view of the narrowband MLE for a scatterer moving at 1 m/s and a periodic transmitted waveform consisting of eight pulses, with the delay d equal to zero. The axial resolution is degraded in comparison with the wideband point MLE. The z axis describes initial scatterer position, and it is the resolution of scatterers with different initial positions that is degraded. In addition, a nearly full height subsidiary velocity peak is present.

The expected receiver output is now shown in Fig. 10 as a function of scatterer velocity. For a point target the two dimensional plot is computed by assuming that the initial pulse delay

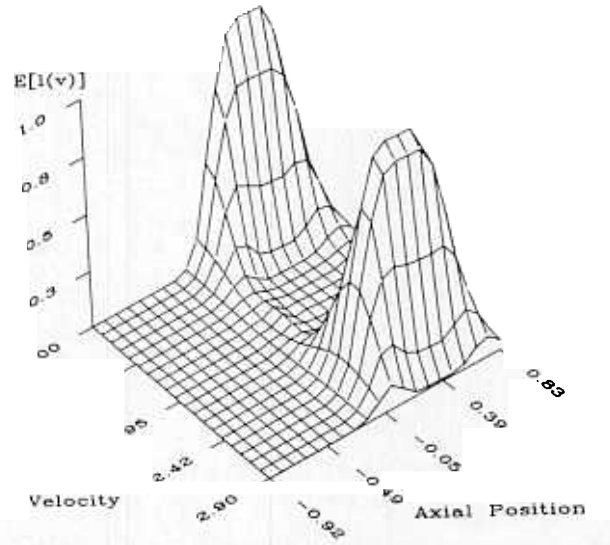

Fig. 9. Expected narrowband MLE output, using eight transmitted pulses. Velocity, v, shown in m/s and axial position, z, in mm.

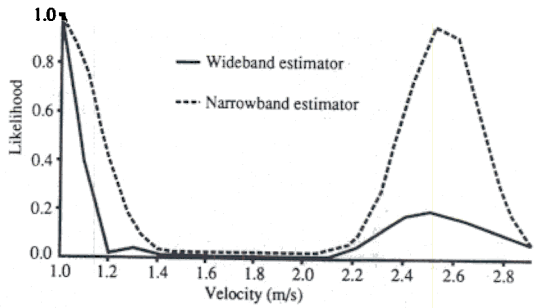

Fig. 10. Comparison of the expected output of the wideband point MLE and narrowband MLE.

d corresponds to the axial location of the target. Therefore, it represents the $z = 0$ axis of the three dimensional plot. Fig. 10 illustrates the difference in performance using the narrowband MLE and the wideband point MLE for an eight-pulse burst, and a scatterer moving at 1 m/s. We observe that global accuracy as defined by the width of the mainlobe and height of subsidiary peaks improves with the wideband point MLE.

The Effect of the Center Frequency: Equation (15) showed that the variance of the wideband point MLE can also be reduced by increasing the signal bandwidth or increasing the center frequency. Fig. 11 shows that the use of a higher center frequency also improves the *global* estimator performance, and magnifies the differences between the narrowband and wideband MLE. The scatterer velocity was 0.2 m/s in this case and a thirty five pulse train with a pulse repetition period of 128 us was used. This corresponds to the experimental conditions considered in Part Two of this paper [19]. The difference in performance would be more significant with a higher scatterer velocity.

B. Expected Output of the Wideband Point MLE with a Range Spread Target

The performance of the estimator derived under the SFPT approximation is now considered for a range spread target, where the model for the received signal from such a target is presented in Appendix A. The target is only range spread but

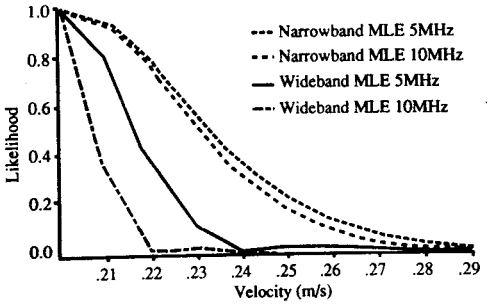

Fig. 11. Effect of center frequency on the expected estimator output.

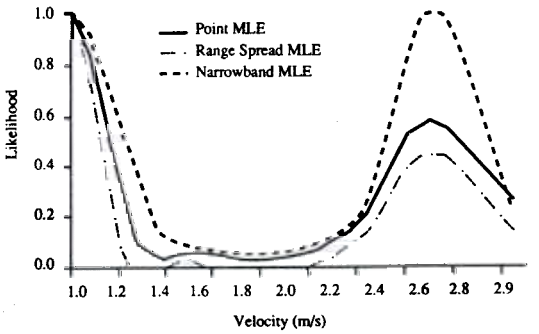

Fig. 12. Comparison of the expected output of the wideband range spread MLE, wideband point MLE and narrowband MLE.

not doubly spread, and therefore the velocity must be uniform throughout the sample volume. Using the spread target ambiguity function as defined in (31) and (32), and evaluating $d = d'$, the expected value is given by

$$\mathcal{E}\{l(v)\} = E_r \int_{cd/2-M}^{cd/2+M} \left| \sum_k \exp\left[j\sigma kT(v-\beta)\right] \cdot R_s[d - 2z/c + 2kT(v-\beta)/c)] \right|^2 dz. \quad (37)$$

Note that evaluation of this expression is equivalent to integrating the three dimensional ambiguity function over the axial dimension. For each axial delay, d, of the signal, we then obtain the ambiguity function for a wideband range spread target. The integration of (37) over target positions, denoted by z, reduces the slope of the estimator output (decreases local accuracy) for a range spread target in comparison with a point target. In addition, it is easily shown from (37) that the integral over the spread target increases the height of the subsidiary velocity peaks in comparison with (33). The peaks remain much smaller than those obtained using the narrowband estimator, however. Using a train of four Gaussian pulses with standard deviation of $300/\sqrt{2}$ ns, the ratio of the first subsidiary peak to the main peak is given by 0.791 for a spread target, compared with the point target result of 0.349.

Using (37), it can again be shown that the performance can be improved by increasing the signal bandwidth or the data window. With an increase in either parameter, the slope of the function for $v = \beta$ increases, and the width of the mainlobe decreases significantly. In addition, the height of the subsidiary peaks decreases dramatically.

C. Expected Value of Wideband Range Spread MLE with a Range Spread Target

The expected value of the wideband range spread MLE in the presence of a range spread target is derived in Ferrara [10], where the range spread target model is discussed in Appendix A. This evaluation again requires the spread ambiguity function, as described in (31) and (32). Letting $d = d'$, $\tau = t - u$, and using g as the difference in the transmitted pulse indices, the expected value is given by

$$\mathcal{E}\{l(v)\} = E_r \int_{-\infty}^{\infty} \mathcal{F}\left\{ \sum_g w_1(g) w_2(g) R_s(\tau - gT[1 + 2\beta/c]) \exp\left[j\sigma\beta\tau\right] \right\} \cdot \left[\frac{\mathcal{F}\left\{ E_r \sum_g w_2(g) R_s(\tau - gT[1 + 2v/c]) \exp\left[-j\sigma v\tau\right] \right\}}{N_o + \mathcal{F}\left\{ E_r \sum_g w_2(g) R_s(\tau - gT[1 + 2v/c]) \exp\left[-j\sigma v\tau\right] \right\}} \right] dw. \quad (38)$$

Fig. 12 shows the evaluation of (38) in comparison with the wideband point MLE for a scatterer velocity of 1.0 m/s using a pulse train of eight pulses and an SNR of 10 dB. The correlation window, $w_2(g)$, is assumed to be constant as a function of g for this short pulse train. The predicted difference in resolution and variance is significant. The slope of the function for $\beta = v$ is increased in comparison with the wideband point MLE in the presence of a range spread target. It can also be shown that the performance of this estimator improves with an increased data window, or increased signal bandwidth. As the data window or bandwidth increases, the slope for $\beta = v$ increases, the width of the mainlobe decreases, and the height of subsidiary peaks decreases.

Height of Subsidiary Peaks: Equation (38) has been evaluated numerically to determine the height of subsidiary peaks. The ratio of the height of the first subsidiary peak to the main peak for a train of four Gaussian pulses with standard deviation of $300/\sqrt{2}$ ns and signal to noise ratio of 10 dB is given by 0.656. The relative height is therefore decreased using the wideband range spread MLE in comparison with the ratio 0.791 which was obtained for the wideband point MLE in the presence of a spread target.

VII. Conclusion

For a proposed use of a wideband transmitted signal, estimation strategies have been developed to utilize the change in scatterer position and the change in frequency of the returned signal. The performance of these strategies was then evaluated, and compared to alternative estimation strategies.

The bound on the variance of the wideband MLE was shown to be smaller than an estimator which only uses phase or delay information. This decrease is due to use of the maximum possible data window and depends on the sum of the two terms resulting from the estimate of the phase and delay. The data window can be optimized for *each* axial region, producing the coherent summation of the maximum number of pulses, possi-

bly based upon an initial evaluation of the correlation of the received signal from this region.

Similarly, evaluation of the expected estimator output showed that the velocity resolution, as defined by the width of the mainlobe, was improved by the use of the wideband strategies. In addition, the height of the subsidiary velocity peaks was shown to be lowered using these strategies. This leads to a reduction in velocity aliasing as compared to current narrowband strategies. The significant reduction of these peaks also provides the opportunity for a future evaluation of alternative nonperiodic signaling schemes. Also, with this reduction, a transmitted signal with an increased center frequency can be used to produce a further performance improvement.

Within the new proposed strategies, it has been shown that the performance of the wideband range spread MLE is superior to the wideband point MLE in the presence of a range spread target. At the cost of an increase in estimator complexity, the bound upon the variance is reduced, and the height of subsidiary peaks is reduced.

The use of a temporally short transmitted signal permits higher levels of peak signal power to be used, while the use of temporally long wideband or narrowband signals requires a reduction in peak transmitted power. This high peak power and short pulse duration maximize the received energy available for the velocity estimate of each small scattering region, and may decrease the received clutter.

Using the wideband transmitted signal and the tracking nature of the estimator, the velocity of each small region of scatterers can be estimated, and therefore the spatial-velocity profile can be estimated across the vessel. The mean velocity and velocity distribution for each spatial location can then be estimated. This velocity distribution within each spatial volume is estimated using the peak magnitude and width of the likelihood function, $l(v)$.

The use of the wideband maximum likelihood estimator provides the potential for further optimization of signal processing for each spatial volume in several ways: deconvolution of the transit time effect for each region of scatterers, optimization of the data window for each individual estimate, and the averaging of subsequent estimates over an optimal time interval.

Appendix A
Simplified Signal Models

In order to clarify the analysis, simplified versions of the model for the received signal are used. The general equation for the received signal is given by (2).

Slowly Fluctuating Point Target Approximation (SFPT)

The slowly fluctuating point target approximation (SFPT), which is frequently used in the derivation of radar structures, requires several assumptions. First, the velocity must be approximately uniform within the sample volume. Second, the effect of lateral beam modulation cannot be significant, since this also produces target fluctuation. Finally, the point target approximation requires the axial dimension of the target to be small in comparison with the distance from the target to the transducer. Using these approximations the received signal is given by

$$r'(t) \approx \sqrt{E_t} \sum_i A_i b(r_i) \sum_k s'[t - 2z/c - kT\{1 + 2\beta/c\}] \exp[-j\sigma(z + \beta t)] \quad (39)$$

with the axial coordinate of the point target denoted by z, and the axial velocity by β.

Range Spread Target

If the target is approximated as a nonfluctuating range spread target, the received signal is given by

$$r'(t) \approx \sqrt{E_t} \sum_i A_i b(r_i) \sum_k s'[t - 2z_i/c - kT\{1 + 2\beta/c\}] \cdot \exp[-j\sigma(z_i + \beta t)]. \quad (40)$$

The effect of target fluctuation on the autocorrelation of this signal may be summarized by the window $w_2(g)$.

Appendix B
Wideband Point MLE

The wideband maximum likelihood estimator is derived under the SFPT model presented in Appendix A. In order to detect the signal in the presence of noise, let us define the received signal under assumptions H_o in which the signal is present, and H_1 in which the signal is absent. The received signal envelope in the presence of noise is denoted $r'(t)$ and consists of a signal, $\bar{r}(t)$, plus band limited white noise, $w'(t)$. Under the two assumptions

$$H_o\colon\ r'(t) = \bar{r}(t) + w'(t) \quad (41)$$

$$H_1\colon\ r'(t) = w'(t). \quad (42)$$

In order to find the sufficient statistic in this case, we set d, the delay of the received signal and v, the axial velocity of the receiver, equal to zero to simplify the algebra involved. We expand $r'(t)$ as a complete orthonormal set of functions with statistically independent coefficients and choose $s'(t)$ as the first orthonormal function.

$$r_1 = \int_0^T r'(t)\{s'^*(t)\}\,dt$$

$$w_1 = \int_0^T w'(t)\{s'^*(t)\}\,dt$$

where

$$H_o\colon\ r_1 \sim CN(0, N_o)$$

$$H_1\colon\ r_1 \sim CN(0, N_o + \sigma_a^2)$$

in which CN denotes the complex normal distribution.

The likelihood ratio for this case is then given by the following expression:

$$\frac{Pr_{1|H_1}(R_1|H_1)}{Pr_{1|H_0}(R_1|H_0)} = \frac{[\pi(2\sigma_a^2 + N_o)]^{-1} \exp -[|R_1|^2/(2\sigma_a^2 + N_o)]}{1/\pi N_o(\exp - [|R_1|^2/(N_o)])} \quad (45)$$

Therefore we can consider $|R_1|^2 \geq k_2$ as our likelihood test and $|R_1|^2$ as our likelihood function. Thus the MLE for axial velocity would be the maximum of $|R_1|^2$ over all v. Assuming the signal s to consist of the sum of short pulses separated by a long period T, the sufficient statistic would then be

$$R_1 = \sum_k \int^{\infty} r'(t)\, s'^*(t - kT)\,dt. \quad (46)$$

Returning to the more general case, let v and d take nonzero values.

$$R_1 = \sum_k \int_{-\infty}^{\infty} r'(t)\, s'^*(t - d - kT[\quad + 2v/c]) \cdot \exp[j\sigma v t]\, dt. \tag{47}$$

The likelihood $l(v)$ is then given by

$$l(v) = \left| \sum_k \int_{-\infty}^{\infty} r'(t)\, s'^*(t - d - kT[1 + 2v/c]) \exp[j\sigma v t]\, dt \right|^2. \tag{48}$$

where

$$H(w) = \mathfrak{F}\{h'(t - u; v)\}$$

and

$$S_r(w) = \mathfrak{F}\left\{ E_r \sum_g w_2(g) \exp\left[-(t - u - gT\mu)^2/2G_t\right] \cdot \exp\left[-j\sigma v(t - u)\right] \right\}$$

Therefore $H(w) = S_r(w)/(N_o + S_r(w))$. Under these conditions, the filter is given by

$$h'(t - u; v) = \mathfrak{F}^{-1}\left[\frac{\mathfrak{F}\left\{ \quad + 2v/c))^2/2G_t\right] \exp\ -j\sigma v(t - u)]\right\}}{N_o + \mathfrak{F}\ E_r \sum_g w_2(g) \exp\ -(t - u - gT(\quad + 2v/c))^2/2G_t] \exp[-j\sigma v(t - u)]} \right]$$

Appendix C
Derivation of the Wideband Range Spread MLE

Using the model for a range spread target presented in Appendix A, the wideband range spread MLE is derived. If the data window is short with respect to the true autocorrelation of the underlying process, the function must be evaluated numerically. The effect of the limited signal correlation is described by a window, $w_2(g)$, over the difference in the transmitted pulse indices, denoted by g. The filter is derived for a simplified case in which the data window is very long and can be approximated as an infinite interval, and the envelope of the transmitted signal is Gaussian with variance G_t. In this situation, the autocorrelation can be rewritten as

$$R_r(t, u) = \sum_{g=-\infty}^{\infty} E_r w_2(g) \exp\left[-(t - u - gT(\quad + 2v/c))^2/2G_t\right] \exp[-j\sigma v(t - u)]. \tag{49}$$

where

$$E_r = \sigma_a^2\, \mathfrak{W}\bar{n}\pi E_t \int_0^{R'} rb[r]^2\, dr \tag{50}$$

and $\mathfrak{W}$, σ_a^2, and $\bar{n}$ were defined in Section III. The autocorrelation is zero outside of the limits of $w_2(g)$. If the data window can be approximated as infinite with respect to $w_2(g)$, the filter $h'(t - u; v)$ can be derived using the Fourier transform. Letting $\mu = (1 + 2v/c)$ and rewriting (5),

$$N_o \cdot h'[t - u; v] + \int_{-\infty}^{\infty} h'[t - x; v] E_r \sum_g w_2(g) \cdot \exp[$$

$$= E_r \sum_m w_2(m) \exp \cdot \exp\left[-j\sigma v(t - u)\right].$$

This quantity can be Fourier transformed as follows:

$$N_o H(w) + H(w) S_r(w) = S_r(w) \tag{52}$$

Appendix D
Bound on the Variance of the Wideband Point MLE

It is important to note that the quantity to be estimated is the MLE of v at each value of z. The problem is not the joint estimation of v and z. Following the method described in Van Trees [11], we can calculate the bound of the variance in the unbiased case using

$$\text{var}[\hat{v} - v] \geq \left\{ -\mathcal{E}\left[\partial^2(c' \cdot l(v))/\partial v^2\right] \right\}^{-1} \tag{54}$$

where $c' = 1/N_o(E_r/[E_r + N_o])$. Therefore we must calculate $\mathcal{E}[\partial^2(c' \cdot l(v)/\partial v^2]$. Using (6) for the likelihood, and defining $r_k'(t)$ as the received signal from the kth transmitted pulse, the denominator of (54) becomes

$$\mathcal{E}\left\{\partial^2(c' \cdot l(v))/\partial v^2\right\} = 2c'\, \text{Re} \int \int_{-\infty}^{\infty} \sum_k \sum_l \mathcal{E}[r_k'(t) r_l'^*(u)] \cdot \left\{ \partial/\partial v[s'^*(t - d - kT - \phi_k v) \exp[j\sigma v t]] \cdot \partial/\partial v[s'(u - d - lT - \phi_l v) \exp[-j\sigma v u)] + s'^*(t - d - kT - \phi_k v) \exp[j\sigma v t] \partial^2/\partial v^2[s'(u - d - lT - \phi_l v) \exp(-j\sigma v u)] \right\} dt\, du \tag{55}$$

Consider the received signal to be generated by a slowly fluctuating point scatterer. In order to evaluate the local performance, we let $z = cd/2$ and evaluate the axial scatterer velocity at v. Under these conditions the autocorrelation can be de-

The presence of an axial velocity gradient requires imposition of an axial window $a(u)$. Although the preceding simplified analysis used an infinite data window, a practical estimator requires a finite window. This is implemented using finite limits of integration and a data window $w_1(t - u)$, and therefore the likelihood of an axial velocity, v, is given by (9).

scribed by the following expression:

$$\mathcal{E}\left[r_k'(t)r_l'^*(u)\right]\Big|_{z=cd/2}$$
$$= 2E_r s'(t - d - kT - \phi_k v)s'^*(u - d - lT - \phi_l v)$$
$$\cdot \exp\left[-j\sigma v(t-u)\right] + N_o\delta(t-u). \quad (56)$$

If the attenuation is negligible, the complex envelope $s'(\cdot)$ is real, the resulting expression for the bound on the variance is given by (15).

References

[1] B. A. J. Angelson, "Instantaneous frequency, mean frequency, and variance of mean frequency estimators for ultrasonic blood velocity Doppler signals," *IEEE Trans. Biomed. Eng.*, vol. BME-28, no. 11, pp. 733–741, Nov. 1981.

[2] P. Atkinson, and J. P. Woodcock, *Doppler Ultrasound and Its Use in Clinical Measurement.* New York: Academic Press, 1982.

[3] M. Azimi, and A. C. Kak, "An analytical study of Doppler ultrasound systems," *Ultrason. Imaging*, vol. 7, pp. 1–48, 1985.

[4] W. R. Brody, "Theoretical analysis of the CW Doppler ultrasonic flowmeter," Ph.D. dissertation, Stanford Univ., 1974.

[5] O. Bonnefous, and P. Pesque, "Time domain formulation of pulse-Doppler ultrasound and blood velocity estimators by cross correlation," *Ultrason. Imaging*, vol. 8, pp. 73–85, 1986.

[6] P. M. Embree, and W. T. Mayo, "Ultrasonic M-Mode RF display technique with application to flow visualization," *SPIE Int. Symp. Pattern Recog. Acoust. Imaging*, vol. 768, 1987.

[7] P. M. Embree, "The accurate ultrasonic measurement of the volume flow of blood by time domain correlation," Ph.D. Dissertation, Univ. Illinois, Urbana-Champaign, 1986.

[8] S. G. Foster, "A pulsed ultrasonic flowmeter employing time domain methods," Ph.D. dissertation, Univ. Illinois, Urbana-Champaign, 1985.

[9] L. Mo, and R. Cobbold, "A stochastic model of the backscattered Doppler ultrasound from blood," *IEEE Trans. Biomed. Eng.*, vol. BME-33, no. 1, pp. 20–27, Jan. 1986.

[10] K. W. Ferrara, "Wideband strategies for blood velocity estimation using ultrasound," Ph.D. Dissertation, Univ. California, Davis, 1989.

[11] Holland, Stephen Kerry. "Estimation of blood flow parameters using pulse Doppler ultrasound with corrections for spectral broadening," Ph.D. Dissertation, Yale Univ., New Haven, CT, 1985.

[12] H. L. Van Trees, *Detection, Estimation and Modulation Theory, Part III.* New York: Wiley, 1971.

[13] M. Olinger, "Ultrasonic blood flow imaging using correlation processing," Ph.D. Dissertation, Michigan State Univ., E. Lansing, MI, 1981.

[14] C. W. Helstrom, *Statistical Theory of Signal Detection.* London: Pergamon Press, 1960.

[15] E. J. Kelly, and R. P. Wishner, R. P. "Matched filter theory for high-velocity, accelerating targets," *IEEE Trans. Mil. Electron.*, pp. 56–68, Jan. 1964.

[16] A. W. Rihaczek, "Delay-Doppler ambiguity function for wideband signals," *IEEE Trans. Aerosp. Electron. Syst.*, vol. AES-3, no. 4, pp. 705–711, July 1967.

[17] A. W. Rihaczek, "Radar resolution of moving targets," *IEEE Trans. Inform. Theory*, vol. IT-13, no. 1, pp. 51–56, Jan. 1967.

[18] P. M. Woodward, *Probability and Information Theory, with Applications to Radar.* London: Pergamon 1964.

[19] K. W. Ferrara and V. R. Algazi, "A new wideband spread target maximum likelihood estimator for blood velocity estimation—Part II: Evaluation of estimators with experimental data," *IEEE Trans. Ultrason. Ferroelec. Freq. Contr.*, vol. 38, no. 1, pp. 17–26, Jan. 1991.

Katherine W. Ferrara (M'87) received the B.S. degree in physical therapy from the University of Pittsburgh, Pittsburgh, PA, in 1976, the B.S. and M.S. in electrical engineering from the California State University, Sacramento, in 1982 and 1983, respectively, and the Ph.D. degree in electrical engineering and computer science from the University of California, Davis, in 1989.

From 1976 to 1980, she practiced physical therapy at the Children's Hospital of Akron, and the Home for Crippled Children, Pittsburgh, PA. From 1983 to 1988, she worked for Sound Imaging, Inc., Folsom, CA, and for General Electric Medical Systems, Rancho Cordova, CA, in the areas of magnetic resonance and ultrasonic imaging. She is currently an Assistant Professor in the Department of Electrical and Electronic Engineering at the California State University, Sacramento. Her research interests are in the fields of signal and image processing, and biomedical engineering.

Dr. Ferrara is a member of Tau Beta Pi and Sigma Xi.

V. Ralph Algazi (M'58–SM'84) received the Ingenieur Radio degree from the Ecole Superieure d'Electricite de Paris, Paris, France, in 1952, and the M.S. and Ph.D. degrees in electrical engineering from the Massachusetts Institute of Technology, Cambridge, in 1955 and 1963, respectively.

From 1955 to 1959, he worked for Feedback Controls, Inc., Natick, MA, and for Westinghouse, Pittsburgh, PA. From 1959 to 1963, he was a Research and Teaching Assistant at M.I.T. Since 1965, he has been with the Department of Electrical Engineering and Computer Science at the University of California, Davis, and served as Chair of the Department from 1975 to 1986. He is now the Director of CIPIC, the Center for Image Processing and Integrated Computing, a multidisciplinary research center at the University of California, Davis. His current interests are in the areas of signal processing, digital picture processing, computer vision, and engineering applications of human perception.

Dr. Algazi is a member of Tau Beta Pi, Sigma Xi, ASEE, SPIE, and AAAS.